Observations of iodine monoxide over three summers at the Indian Antarctic bases, Bharati and Maitri

Anoop S. Mahajan[1*], Mriganka S. Biswas[1,2], Steffen Beirle[3], Thomas Wagner[3], Anja Schönhardt[4], Nuria Benavent[5] and Alfonso Saiz-Lopez[5]

[1]Centre for Climate Change Research, Indian Institute of Tropical Meteorology, Ministry of Earth Sciences, Pune, 411008 India.

[2]Savitribai Phule Pune University, Pune, 411008 India.

[3]Max-Planck-Institut für Chemie (MPI-C), Satellitenfernerkundung, 55128 Mainz, Germany

[4]Institute of Environmental Physics, Department of Physics and Electrical Engineering, University of Bremen, Bremen, 330440 Germany.

[5]Department of Atmospheric Chemistry and Climate, Institute of Physical Chemistry Rocasolano, CSIC, Madrid 28006, Spain

* corresponding author: Anoop S. Mahajan (anoop@tropmet.res.in)

Abstract

Iodine plays a vital role in oxidation chemistry over Antarctica, with past observations showing highly elevated levels of iodine oxide (IO) leading to severe depletion of boundary layer ozone in West Antarctica. Here, we present multi axis differential absorption spectroscopy (MAX-DOAS) based observations of IO over three summers (2015-2017) at the Indian Antarctic bases, Bharati and Maitri. IO was observed during all the campaigns, with mixing ratios below 2 pptv for the three summers, which are lower than the peak levels observed in West Antarctica. This suggests that sources in West Antarctica are different or stronger than sources of iodine compounds in East Antarctica, the nature of which are still uncertain. Vertical profiles estimated using a profile retrieval algorithm showed decreasing gradients, with a peak in the lower boundary layer. The ground-based instrument retrieved vertical column densities (VCDs) were approximately a factor of three-five higher than the VCDs reported using satellite-based instruments, which is most likely related to the sensitivities of the measurement techniques. Airmass back-trajectory analysis failed to highlight a source region, with most of the airmasses coming from coastal or continental regions. This study highlights the variation in iodine chemistry in different regions in Antarctica and the importance of a long-term dataset to validate models estimating the impacts of iodine chemistry.

Keywords: Iodine; Antarctica; halogens; DOAS

1. Introduction

Reactive halogen species (RHS) have been shown to play a critical role in causing ozone depletion events in the polar boundary layer (BL) (Barrie et al., 1988; Bottenheim et al., 1986; Kreher et al., 1997; Oltmans and Komhyr, 1986) and could contribute to new particle formation in this remote environment (Allan et al., 2015; Atkinson et al., 2012; O'Dowd et al., 2004). Observations of RHS have been made in the Antarctic BL for almost two decades. Early observations focused on bromine oxide (BrO), the presence of which was observed in the Antarctic using ground based instruments (Kreher et al., 1997) and via satellites (Hollwedel et al., 2004). The presence of iodine oxide (IO) in the Antarctic atmosphere was also confirmed through integrated column measurements from the ground (Frieß et al., 2001). Later, year-long ground-based observations of RHS made at Halley Bay showed the critical role that bromine and iodine compounds play in regulating the oxidizing capacity, causing ozone depletion and new particle formation in the Antarctic BL (Saiz-Lopez et al., 2007a). These ground-based observations showed that both IO and BrO, are present at elevated concentrations (from 1 pptv to as high as 20 pptv) in certain parts of the Antarctic BL, and show a significant seasonal variation peaking in the spring, with elevated concentrations observed through the summer (Saiz-Lopez et al., 2008). Satellite-based observations of both IO and BrO reported a similar annual cycle, although with large geographical differences (Hollwedel et al., 2004; Richter et al., 2002; Saiz-Lopez et al., 2007b; Schönhardt et al., 2008, 2012; Theys et al., 2011; Wagner et al., 2001). These satellite observations have been validated by ground-based observations, although most of them have hitherto focused around the Weddell Sea (Atkinson et al., 2012; Buys et al., 2013; Frieß et al., 2001, 2010; Saiz-Lopez et al., 2007a, 2008). Previous studies show that similar levels of BrO have been observed between the Arctic and Antarctic while much lower levels of atmospheric iodine have been reported in the

57 Arctic compared to the Antarctic (Hönninger et al., 2004; Raso et al., 2017; Schönhardt et al.,

58 2008; Tuckermann et al., 1997). The satellite observations also show a difference in the

59 geographical distribution of IO over Antarctica, with the Weddell sea being an iodine hotspot, the

60 reasons for which are still not completely clear (Saiz-Lopez and Blaszczak-boxe, 2016). Ground-

61 based observations have also been made at McMurdo Sound, near the Ross Sea, where lower

62 concentrations of IO were observed (Hay, 2010). Additional observations over the 2011-2012

63 summer were made at Dumont d'Urville using a cavity enhanced absorption spectroscopy based

64 instrument and showed a maximum of 0.15 pptv of IO (Grilli et al., 2013). However, observations

65 of IO have not been reported in the Indian Ocean sector of the Antarctic peninsula to date (Saiz-

66 Lopez et al., 2012; Saiz-Lopez and von Glasow, 2012).

67 Ground based observations at Halley Bay and in the Weddell Sea suggest that the main source of

68 iodine compounds is the sea ice region based on observations of iodocarbons and back trajectory

69 analysis (Atkinson et al., 2012; Saiz-Lopez et al., 2007a). Other studies have also measured

70 iodocarbons in Antarctica, although their levels are too low to explain the high levels observed in

71 the Weddell Sea region (Carpenter et al., 2007; Fogelqvist and Tanhua, 1995; Reifenhäuser and

72 Heumann, 1992). The exact process is still not known, although a mechanism for biologically-

73 induced iodine emissions from sea-ice has been suggested based on the idea that micro-algae

74 (Garrison and Buck, 1989) are the primary source of iodine emissions in this environment (Saiz-

75 Lopez et al., 2015a) with halogen compounds then moving up brine channels in the sea ice to

76 finally get released into the atmosphere. There are further questions regarding the propagation of

77 reactive iodine chemistry across the continent because satellite observations show the presence of

78 IO deep within the Antarctic continent, even as far as the South Pole (Saiz-Lopez et al., 2007b;

79 Schönhardt et al., 2008). However, although enhanced, the observed IO column densities are close

80   to the detection limit of the satellite instrument (~7 x 10^{12} molecules cm^{-2} for a single

81   measurement) and are therefore subject to uncertainties. The study by Frieß et al. (2010) suggested

82   a strong source within the snowpack, which hints at active recycling and re-emission of IO aiding

83   the long transport inland. However, questions remain about why such a source would function

84   only in parts of the continent and why the primary source is different from the Arctic, where much

85   lower peak concentrations are sporadically observed (Mahajan et al., 2010; Saiz-Lopez and

86   Blaszczak-boxe, 2016). To further understand the sources of iodine in the polar environment,

87   understanding the geographical distribution is critical. Satellite observations play a useful role for

88   this, although validation of the satellite observations using ground-based instruments is necessary

89   to ascertain their accuracy to observe IO in the Antarctic troposphere.

90   Questions also remain about the vertical profiles of iodine compounds within and above the

91   Antarctic boundary layer. Modelling based studies using the one-dimensional Tropospheric

92   Halogen Chemistry MOdel (THAMO) have suggested a strong gradient in IO from the surface to

93   the edge of the boundary layer (Saiz-Lopez et al., 2008). Only once in the past have vertical profiles

94   of IO been measured in Antarctica. These measurements were made at McMurdo Sound in East

95   Antarctica (Hay, 2010). Observations over two "golden days" in 2006 and 2007 show surface

96   concentrations of about 1 pptv, decreasing to ~0.2 pptv at about 200 m, before reaching a second

97   maximum of 0.6 pptv at ~700 m. However, models did not reproduce this measured IO vertical

98   profile shape and there are also large uncertainties associated with the a priori (Hay, 2010). In most

99   models, the assumption is that the source of iodine compounds is from the snowpack, with

100 photochemistry in the atmosphere resulting in a steady decrease with altitude. However,

101 considerable challenges remain in reproducing the surface variation and vertical gradients in

102 addition to the geographical distribution (Fernandez et al., 2019). More recent modelling studies

103 combined with aircraft observations suggest that the gradient is not very sharp all the latitudes,

104 with a significant free tropospheric and stratospheric contribution to the total column of IO

105 (Koenig et al., 2020; Saiz-Lopez et al., 2015b), although such observations have still not been done

106 in the Antarctic. One of the main reasons for the uncertainties in models is the lack of consistent

107 measurements of vertical gradients across the world, especially in the Polar Regions, to validate

108 these model simulations.

109 Considering the uncertainties in the satellite observations and questions regarding the sources and

110 vertical and geographical distribution of IO, further observations are necessary. Here we present

111 observations made at two new locations in Antarctica over three summers and compare them with

112 the satellite-based retrievals and past observations.

113

2. Methodology

115 Figure 1 shows the location of the two Indian Antarctic stations, Maitri (11.73 °E , 70.77 °S) and

116 Bharati (76.19 °E, 69.41 °S). The other stations where observations of IO have been reported in

117 the past are also marked on the map. Observations of IO and the oxygen dimer (O_4) were made

118 using the Multi-Axis Differential Optical Absorption Spectroscopy technique (MAX-DOAS) over

119 three summers: February-March 2015 as a part of the 34th Indian Scientific Expedition to

120 Antarctica (ISEA-34), November 2015 – February 2016 as a part of ISEA-35 and January-

121 February 2017 as a part of ISEA-36.

122 Observations at the Maitri station were made over a short span of 9 days (9th March – 17th March

123 2015) and only during ISEA-34. The research station is in the ice-free rocky area on the

124 Schirmacher Oasis. The MAX-DOAS instrument was installed in a summer-time residential

125   container, ~150 m north the station, about 120 m above sea level during the ISEA-34. The scanner

126   unit was mounted on top of the container with the clear line of sight to the horizon. The scanner

127   pointed ~60.0° with respect to magnetic north. The spectrometer unit was kept inside the container,

128   which was temperature controlled. The open ocean is 125 km north of Maitri.

129   Observations at the Bharati station were made for 10 days (9th February-18th February 2015) during

130   ISEA-34, for 63 days (30th November 2015 – 1st February 2016) during ISEA-35 and for 35 days

131   (5th January-11th February 2017) during ISEA-36. The station is located between the Thala Fjord

132   and Quilty Bay, east of the Stornes Peninsula. The MAX-DOAS instrument was installed in a hut

133   on top of a ridge around 200 m south-west of the Bharati station and was approximately 56 m

134   above sea level. The scanner unit was mounted on the wall of the hut and had a clear line of sight

135   to the horizon, pointing -23.2° with respect to the north, overlooking the open ocean. The coastline

136   is within 500 m of the hut, but it becomes ice free from mid-January to late March. Depending on

137   the sea ice conditions, the open ocean is within 8-10 km north from the end of November.

138   The MAX-DOAS instrument (EnviMes) makes use of scattered sunlight along different elevation

139   angles and by combination of several lines of sight including the zenith. The concentration of an

140   absorber in the boundary layer can be obtained either in a first approximation by a simple

141   geometric approach or by simulating the light path with a radiative transfer model taking into

142   account also multiple scattering effects and the correct treatment of the aerosol loading in the

143   atmosphere (Hönninger et al., 2004; Platt and Stutz, 2008; Wagner et al., 2004). The instrument

144   consists of an indoor unit, housing a spectrometer with a spectral resolution of 0.7 nm (UV: 301.20-

145   463.69), which is connected to an outdoor unit, containing a scanning telescope. Discrete elevation

146   angles (1°, 2°, 3°, 5°, 7°, 10°, 20°, 40°, and 90°) were recorded for a total exposure time of 1

147   minute each during all the four campaigns. The spectra were recalibrated before analysis using

148 mercury emission lines recorded at the end of each day. For DOAS retrieval, the QDOAS 3.2

149 software was used (Fayt and Van Roozendael, 2013). For estimation of the O_4 Differential Slant

150 Column Densities (DSCDs), the cross-sections of O_4 (Thalman and Volkamer, 2013) at 293K;

151 NO_2 (Vandaele et al., 1998) at 220 K and 298 K (220 K orthogonalized to 294 K); O_3 (Bogumil et

152 al., 2003) at 223 K and 243 K (orthogonalized to O_3 at 243 K); HCHO (Meller and Moortgat,

153 2000) at 298 K; HONO (Stutz et al., 2000) at 296 K were used in the 351-390 nm window. The

154 cross-sections used for IO retrieval in the 417-440 nm spectral window were: IO (Gómez Martín

155 et al., 2005), NO_2 220 K and 298 K (Vandaele et al., 1997), H_2O (Rothman et al., 2013), O_4

156 (Thalman and Volkamer, 2013) and O_3 (Bogumil et al., 2003). In addition to these cross-sections

157 a ring spectrum (Chance and Spurr, 1997), a second ring spectrum following Wagner et al. (2009),

158 and the 3rd order polynomial were used for both windows. The zenith spectrum from each scan

159 was used as a reference to remove contribution from possible free tropospheric or stratospheric

160 absorption. An example of a DOAS fit for O_4 and IO are given in Figure S1. Surface mixing ratios

161 and the total vertical column densities (VCDs) were retrieved from the MAX-DOAS DSCDs of

162 IO and O_4 by employing the Mainz Profile Algorithm (MAPA) (Beirle et al., 2018). Only

163 observations with solar zenith angles (SZA) less than 75° were used for the profile retrievals due

164 to the large path lengths through the stratosphere for high SZA angles. This algorithm uses a two-

165 step approach to determine the trace gas vertical profiles. In the first step, the aerosol profiles are

166 retrieved using the measured O_4 DSCDs. A Monte Carlo approach is utilized to identify the best

167 ensemble of the forward model parameters (column parameters (c) (VCD for trace gases and

168 aerosol optical depth for aerosol), height parameter (h) and shape parameter (s)), which fit the

169 measured O_4 DSCDs for the sequence of elevation angles. In the second step, the aerosol profiles

170 retrieved from the O_4 inversion are used as an input to retrieve similar model parameters (c, h, and

171 s) for IO. The state of the atmosphere was calculated using the pressure and temperature profiles

172 observed by the in-situ radiosondes, which were launched once a week at both stations. An

173 angstrom exponent of 1 was used for the difference in the retrieval wavelengths as per observations

174 made at Bharati in the past (Prakash Chaubey et al., 2011). Within MAPA, the differential air mass

175 factors (AMFs) are calculated offline with the radiative transfer model McArtim (Deutschmann et

176 al., 2011) for fixed nodes for each parameter and stored as a lookup table (LUT) for quick analysis.

177 To assess the quality of the retrievals, MAPA provides "valid", "warning" or "error" flags for each

178 measurement sequence, which are calculated based on pre-defined thresholds for various fit

179 parameters. For further details about MAPA, please refer to the description paper by Beirle et al.

180 (2018). Additionally, MAPA provides the option to use a scaling factor for significant mismatch

181 between the modelled and measured O_4 DSCDs, which has been shown to be close to 0.8 in the

182 past (Wagner et al., 2019). Using the variable option, where the model estimates the scaling factor,

183 which ranged between 0.75 and 0.9. Therefore, a scaling factor of 0.8 was applied for all the

184 campaigns.

185 We also make use of the IO vertical column densies retrieved using the SCanning Imaging

186 Absorption spectroMeter for Atmospheric CHartographY (SCIAMACHY), a UV-vis-NIR

187 spectrometer onboard the ENVISAT satellite (Burrows et al., 1995). Observations from

188 SCIAMACHY stopped due to instrumental problems in April 2012. Here we make use of the mean

189 from 2004-2011 to look at the geographical distribution and compare it with the ground-based

190 observations made during the study period. Further details about the IO retrieval algorithm and the

191 SCIAMACHY instrumental setup can be found elsewhere (Schönhardt et al., 2008, 2012).

192

3. Results and Discussion

3.1 Meteorological parameters

Figure 2 shows the 5-day back-trajectories arriving every hour at the two stations at a height of 10 m on the days that the DOAS measurements were conducted as a part of the three ISEA expeditions. The back-trajectories were calculated using the HYbrid Single-Particle Lagrangian Integrated Trajectory (HYSPLIT) using the using the EDAS-40 km database (Draxler and Rolph, 2003). The trajectories show that the airmasses sampled throughout the three expeditions were from either a remote oceanic region, coastal Antarctica, or the continental shelf. In general, most of the trajectories show that the airmasses had travelled over hundreds of kilometres over the last five days. For the local meteorological conditions, Figure 3 (top panels) show the wind direction at the Bharati station. Most of the time, the wind was from the ocean, with the winds coming from the north-west sector and a few instances of northern and north eastern winds (although during ISEA-34 the winds were mostly from east to north-east). This was during all the three expeditions at the Bharati station. The wind speed was mostly below 20 knots (~10 m s^{-1}) for all the campaigns, although periods of high winds were observed during ISEA-35 and ISEA-36, which were of a longer duration than ISEA-34. The temperature at the station hovered between -5 °C and +5 °C, through the summer period, with higher values closer to noon (Figure 3, middle panels). The humidity fluctuated from 40% to above 90%. The radiation followed a clear diurnal pattern, with the highest values seen around local noon and minima at local midnight. Considering that this region experiences continuous light for 24 hours, the radiation also showed a non-zero minima between November to January (Figure 3, bottom panels). However, in February, a clear night-time is seen in the radiation data. Finally, a measure of the cloudiness was also tracked using visual full sky cloud cover observations. Any cloud cover of more than 30% was considered to be cloudy

216   (cloud flag value of 1), which helps in filtering the MAX-DOAS observations. In addition to the

217   visual inspection of the sky, which was performed once an hour, a second cloud index was

218   calculated based on the ratios of the radiances at 320 nm and 440 nm from the 3° and zenith spectra

219   (Mahajan et al., 2012; Wagner et al., 2014). Both manual and radiance-based indices showed a

220   close match, indicating that cloudy conditions were well discerned by the cloud index calculation.

221   Meteorological data was unfortunately not available at the Maitri station.

222   **3.2 Differential Slant Column Densities (DSCDs)**

223   Figure 4 shows the observed O_4 DSCDs at different elevation angles for all the campaigns. O_4

224   DSCDs were found to be higher at lower elevation angles, as expected, which is because the O_4

225   concentration is proportional to the square of the oxygen pressure and thus increases towards the

226   surface. This also suggests that the aerosol loading was low in the atmosphere. Photons travel

227   longer paths at lower elevation angles and interact more with tropospheric absorbing species before

228   reaching the instrument resulting in a decreasing profile with increasing elevation angles. The

229   average residual root mean square (RMS) and 2σ detection limit for the O_4 DSCDs were 4.46×10^{-4}

230   (range: $1.56\text{-}10.01\times10^{-4}$) and 2.11×10^{42} molecules^2 cm^{-5} (range: $0.72\text{-}4.66 \times 10^{42}$ molecules^2

231   cm$^{-5)}$, respectively (Figure 4). The O_4 DSCDs were then used to estimate the aerosol profiles and

232   hence the IO mixing ratios, as described earlier in section 2.

233   Figure 5 shows the observed IO DSCDs at different elevation angles for all the campaigns. The

234   IO DSCDs were found to be higher at lower elevation angles, which indicates a decreasing gradient

235   in the IO vertical profile. The residual RMS was in the $1.15\text{-}9.73\times10^{-4}$ range (mean: 3.46×10^{-4}),

236   resulting in 2σ IO DSCD detection limits of 6.57×10^{12} to 5.71×10^{13} molecules cm^{-2} (mean

237   1.88×10^{13} molecules cm^{-2}) (Figure 5). For several days, only the lowermost elevation angles were

238 found to be above the two-sigma detection limit of the instrument. Higher IO DSCDs were

239 observed at high SZAs, which is related to an increase in the path length. However, only

240 observations with SZA<75° were used to estimate the vertical profiles and surface mixing ratios

241 using the aerosol profiles derived using the O_4 DSCDs, as described earlier in section 2. A zoomed

242 in view of two example days for both the O_4 and IO DSCDs is shown in Figure S2, which clearly

243 shows the decreasing gradient with increasing elevation angles.

3.3 IO Vertical Column Densities (VCDs) and mixing ratio profiles

245 The O_4 and IO DSCDs were used to retrieve the vertical column densities and the vertical profiles

246 for aerosols and IO. A comparison of the MAX-DOAS observed O_4 DSCDs with the MAPA

247 modelled DSCDs for all the four campaigns are shown in Figure S3, and Figure S4 shows a similar

248 plot for the IO DSCDs. Figure 6 and 7 show the MAPA calculated AODs and IO VCDs,

249 respectively, for all the campaigns. Several datapoints are flagged as error or warnings, with a few

250 scans giving a 'valid' flag. In the case of aerosols, the warning or error flags are mainly for scans

251 which were during cloudy weather (Figure S5 shows the data, which were flagged as 'bad' and

252 'warning' along with the valid scans). As mentioned above, the cloud cover was regularly

253 measured throughout the campaigns as a part of the meteorological observations. In addition to

254 visual observations, we also computed the cloud index following past works based on MAX-

255 DOAS observations (Mahajan et al., 2012; Wagner et al., 2014), which confirmed that the error

256 and warning flags were during cloud cover periods. For the valid scans, the aerosol optical depth

257 (AOD) ranged between 0.002 and 0.016, with a mean value of 0.003 for ISEA-34 at Bharati;

258 between 0.001 and 0.067, with a mean value of 0.011 for ISEA-34 at Maitri; between 0.001 and

259 1.866, with a mean value of 0.037 for ISEA-35 at Bharati; and between 0.001 and 0.878, with a

260 mean value of 0.016 for ISEA-36 at Bharati (Figure 6). The low values are expected considering

261   the pristine conditions in Antarctica, although during a couple of scans elevated levels were

262   observed as demonstrated by the maximum value during ISEA-35 and ISEA-36. In the case of IO,

263   there were far fewer valid retrieved profiles as can be seen in Figure 7 (Figure S6 shows the all

264   scans, including the 'bad' and 'warning'). Only 343 valid total scans were retrieved for the vertical

265   profiles of IO. One of the main reasons is that for most of the scans the IO DSCDs at higher

266   elevation angles are below the detection limit and not enough information is available for the

267   model to retrieve a valid vertical profile. In the case of IO VCDs, there were only two scans that

268   showed a valid flag over the 10-day period during the ISEA-34 campaign at Bharati due to adverse

269   weather conditions leading to mostly cloudy weather. Thus, the mean VCD value of 2.83×10^{12}

270   molecules cm^{-2}, should be treated with some caution. In Maitri during ISEA-34, the IO VCD

271   ranged between 2.37×10^{12} molecules cm^{-2} and 4.25×10^{12} molecules cm^{-2}, with a mean value of

272    $3.40 \pm 0.57 \times 10^{12}$ molecules cm^{-2}. During ISEA-35 at Bharati, which had the highest number of

273   valid scans over the four campaigns, the IO VCDs ranged between 0.01×10^{12} and 5.86×10^{12}

274   molecules cm^{-2}, with a mean value of $2.62 \pm 1.16 \times 10^{12}$ molecules cm^{-2}. During ISEA-36, the IO

275   VCDs ranged between 2.78×10^{12} molecules cm^{-2} and 4.90×10^{12} molecules cm^{-2}, with a mean value

276   of $3.92 \pm 0.79 \times 10^{12}$ molecules cm^{-2} at Bharati.

277   In addition to the VCDs, vertical profiles of aerosols (Figure S7) and IO were estimated using

278   MAPA. Figure 8 shows the typical vertical profiles of IO mixing ratios over the four expeditions.

279   The surface mixing ratios for the valid scans across all the campaigns range between 0.2 and 1.3

280   pptv. The surface (<30 m) concentrations observed at both Maitri and Bharati are lower than

281   observations in the Weddell Sea region, where summer time concentrations exceeding 6 pptv have

282   been reported in the past (Atkinson et al., 2012; Saiz-Lopez et al., 2007a), or at the Neumayer

283   station, where long-term zenith sky DOAS measurements of IO suggest mixing ratios as high as

284 ~10 pptv during the summer (Frieß et al., 2001). It should be noted that although elevated

285 concentrations were observed at Halley, the average summer concentration, measured only 4 m

286 above the snowpack using a Long-Path DOAS instrument, was about 3 pptv, approximately a

287 factor of three higher than the observations at Bharati and Maitri. Considering that the MAX-

288 DOAS retrieved profiles are not very sensitive to the lowermost few meters, this difference is

289 expected. This is because the source of IO is expected to be from the surface and remote sensing

290 estimates have suggested that high IO concentrations in the order of 50 ppbv are present in the

291 snow interstitial air (Frieß et al., 2010), suggesting that snowpack is indeed the source for iodine

292 compounds. If this is the case, a strong gradient would be observed considering the short lifetime

293 of IO in the atmosphere, and hence the MAX-DOAS observations would be lower than the LP-

294 DOAS observations. However, this does not explain the large difference compared to Neumayer,

295 where the estimated value was 10 pptv. Indeed, Maitri is close to Neumayer, and the reasons for

296 the large difference between the two sites remains a mystery. The observations reported in this

297 study are also similar to measurements at McMurdo Sound, near the Ross Sea, where MAX-DOAS

298 observations reported a maximum of 2.6 ± 0.1 pptv with most of the observations below 1 pptv

299 during 2006 and 2007 (Hay, 2010). It should be noted that the surface values were not highly

300 weighted by the a priori. McMurdo Sound is also located in the East Antarctic, which shows lower

301 levels of IO in the satellite estimates (Schönhardt et al., 2008) and in models (Fernandez et al.,

302 2019).

303 Vertical profiles of IO have been reported only once in the past from Antarctica. These

304 measurements were made at McMurdo Sound in East Antarctica (Hay, 2010). IO over two days in

305 2006 and 2007 show typical surface concentrations of ~1 pptv (with a maximum of 2.6 pptv),

306 decreasing to ~0.2 pptv at about 200 m. A second maximum of 0.6 pptv at ~700 m was also

307 observed, but the models do not reproduce this profile shape and the observations were subject to

308 large uncertainties with the vertical profile above 200 m dominated by the a priori (Hay, 2010).

309 During the four campaigns studied here, elevated concentrations, similar to the surface, were

310 usually observed until about 400 m. Above this height, there is a decrease, with the retrievals

311 reducing to below 0.1 pptv (Figure 8). The reducing standard deviations in the profile retrieval

312 with altitude show that all the profiles which reproduce elevated IO close to the ground approach

313 zero for higher altitudes, suggesting that most of the IO is within the lower part of the troposphere.

314 However, this gradient is much more gradual than estimates predicted using the THAMO one-

315 dimensional model at Halley Bay (Saiz-Lopez et al., 2008). In most models, the assumption is that

316 the source is from the snowpack, and hence a strong decreasing gradient with altitude has been

317 predicted (Saiz-Lopez et al., 2008). The gradient of this decrease depends on the photolysis of the

318 higher oxides, and on the recycling of iodine reservoir species on aerosols, both of which have

319 uncertainties. When the gradient was estimated in 2008 (Saiz-Lopez et al., 2008), the photolysis

320 rates for the higher iodine oxides were not available but this has recently been measured in the

321 laboratory (Lewis et al., 2020) and THAMO needs to be updated accordingly. Another important

322 point to consider is that the MAX-DOAS observation-based profile retrievals typically get only a

323 couple of points of information in the boundary layer and are hence not expected to capture this

324 strong decrease.

325 **3.4 Comparison with satellite-based estimates**

326 The satellite-based vertical column densities of IO across the Weddell Sea region, and the region

327 encompassing Bharati and Maitri are shown in Figure 9. The averaged satellite based VCD

328 observations suggest that lower levels of IO are expected at both the Indian bases as compared to

329 places where ground-based observations have been reported in the past, such as Halley Bay and

330 Neumayer. The mean and standard deviation over the eight years of observations for Bharati is 0.6

331 $\pm$ 0.5 $\times 10^{12}$ molecules cm^{-2}, while for Maitri the amount is 0.5 $\pm$ 0.5 $\times 10^{12}$ molecules cm^{-2}, each

332 for the whole time series. For single months the values can be higher: the mean IO VCD for Bharati

333 is 0.8 or 0.4 $\times 10^{12}$ molecules cm^{-2} in December or February, respectively, and 0.6 $\times 10^{12}$ molecules

334 cm^{-2} in March for Maitri. This is lower than mean value of 2.62 $\pm$ 1.16$\times 10^{12}$ molecules cm^{-2}

335 observed at Bharati during ISEA-35, which was the longest dataset available in this study which

336 suggests that the ground-based instruments observe larger VCDs as compared to the satellite based

337 instruments. However, it should be noted that the SCIAMACHY data is an average over all the

338 seasons, and individual daily datapoints as high as 2.1$\times 10^{12}$ molecules cm^{-2} have been observed.

339 Figure 10 shows the timeseries for Bharati and Maitri with daily averages (red dots) as well as

340 monthly averages (blue triangles) for the years 2004 to 2011. Satellite measurements from within

341 500 km around the stations were included in the analysis. It should be mentioned that this spatial

342 averaging could cause introduction of larger uncertainties due to the heterogeneity in the IO

343 distribution, but are necessary to improve the signal to noise.

344 When the whole IO column is constrained to the lower 400 m, the satellite retrieved VCDs translate

345 to a range between 0.6 – 1.3 pptv. The daily satellite VCDs tend to exceed these averaged values

346 and result in mixing ratios as high as 2 pptv. This is similar to the range observed through the four

347 campaigns reported here. However, observations during the spring time were not made over these

348 four campaigns, when emissions of iodine species have been show to peak at Halley Bay (Saiz-

349 Lopez et al., 2007a). During the spring season, values as high as 20 pptv was observed at Halley

350 Bay, a factor of ten higher than during the summer at the Indian stations. However, the satellite

351 observations do not show a large peak over the springtime over both Indian stations. Another

352 outstanding question is whether the satellites are sensitive to the lower 100-200 m, considering the

353 strong gradient in IO. Figure S8 shows the block AMFs for satellite retrievals showing a significant

354 difference between the block AMFs over Antarctica at different albedo values. Over the ice-

355 covered regions in Antarctica, the satellite is sensitive to the lower troposphere as the albedo is

356 usually 0.9 or above. Observations have shown that open water has an albedo of 0.05–0.2 (Jin et

357 al., 2004), whereas the albedo of sea ice ranges between 0.6 and 0.7 for bare ice and 0.8–0.9 for

358 snow-covered ice (Perovich et al., 2002). In the case of Bharati, the Quilty Bay is not ice covered

359 during the summer and hence along the light path in Bharati, the sensitivity of the satellite is much

360 lower. Use of a higher albedo would result in an underestimation of the VCD by the satellite, which

361 is the case when compared to the ground-based instruments. At Mairti this should not be the case

362 considering that Maitri is 125 km inland from the coast, and the ice shelf is less than 1 km from

363 the station along the light path. It should be noted that the MAPA LUTs are calculated for a low

364 surface albedo (5%) and hence, at least for some of the measurements, the surface albedo is

365 probably much higher, especially at Maitri. As far as we understand, the effect of the surface

366 albedo mainly cancels out in the MAX-DOAS analysis, but it could be one possible uncertainty

367 on the retrieval results. Another reason for the discrepancy between the ground based and satellite

368 retrieved VCDs could be the overpass time, which was approximately 09:00 am local time.

369 Although this should not be a large factor during the summer months due to long sunlit hours, and

370 that the numbers given above were averages through the entire campaign for the ground-based

371 observations, measurements at Halley Bay have shown a strong diurnal profile peaking at noon

372 (Saiz-Lopez et al., 2007a). Hence, it is possible that the ground-based observations, which are

373 filtered for SZA>75°, capture higher values than the satellite.

374 Finally, a point to consider is that the satellite data available from SCIAMACHY is for the period

375 of 2004-2011, whereas the MAX-DOAS observations were conducted over three summers from

376 2015. This temporal discrepancy, although small considering the long satellite dataset, could

377 contribute to the difference in the retrieved VCDs. Recent observations of iodine in ice-cores in

378 the Alpine region and over Greenland have shown an increasing trend for atmospheric iodine in

379 the northern hemisphere (Cuevas et al., 2018; Legrand et al., 2018). In the Antarctic only seasonal

380 and geographical variations in halogens in the ice have been studied and no long term dataset is

381 available (Vallelonga et al., 2017). The main cause for this increase is suggested to be an increase

382 in tropospheric ozone, which drives the emission of iodine compounds from the ocean surface

383 through heterogenous chemistry at the ocean interstitial surface (Carpenter et al., 2013). Although

384 questions regarding the strength of this inorganic source in affecting IO concentrations in the

385 Southern Ocean remain (Inamdar et al., 2020; Mahajan et al., 2019), it is possible that the

386 discrepancy between the satellite and ground based data is because of a different time period.

387 However, no increasing trend was observed in the satellite data for the period between 2004-2011

388 (Figure 10), which suggests that a factor of three increase in the VCDs is most likely due to a

389 difference in the measurement technique and sensitivities rather than a change in the emissions.

390

391 **3.5 Airmass origin dependence**

392 Year-long observations at Halley Bay in West Antarctica, which were made using the LP-DOAS

393 instrument, suggested a oceanic primary source (Saiz-Lopez et al., 2007a). The authors showed

394 through the tracking of airmass back-trajectories, which displayed that elevated levels of IO were

395 present in airmasses that passed over the coastal and oceanic regions compared to the airmasses

396 that had only continental exposures. However, even in airmasses that had passed only over the

397 continent for the past five days, the IO levels were still above the detection limit, which suggested

398   that even if the primary source is oceanic, a secondary source from the snow pack contributed to

399   the atmospheric IO. Indeed, subsequent studies have tried to explain the snowpack source through

400   recycling of primary emissions from the ocean (Fernandez et al., 2019) and one study has even

401   suggested a strong snowpack source based on simulated observations (Frieß et al., 2010). Although

402   the levels of IO are much lower than the peak concentrations seen at Halley Bay, we studied the

403   back-trajectories to see if the origin of airmasses lead to a difference in the observed IO levels at

404   both Bharati and Maitri. Considering the short lifetime of reactive iodine compounds in the

405   atmosphere, we calculated the exposure of each HYSPLIT calculated back-trajectory according to

406   the region it passed over the last 12 hours. Depending on where the trajectories spend the most

407   amount of time, they were classified into coastal, continental, and oceanic airmasses. The coastal

408   region was defined as a 0.5° belt along the Antarctic coastline, with regions to the north and south

409   of this belt considered to be oceanic and continental, even though most of them had coastal origin

410   when the 5 day trajectories are considered (Figure S9). Using the profiles which were valid, no

411   clear dependence on the airmass origin was observed. Indeed, most of the data points at both

412   stations corresponded to airmasses which were either coastal or continental (Figure S10) and is

413   representative of the typical wind patterns during the summer season. Thus, using this dataset, it

414   was not possible to draw any conclusions regarding the possible sources of IO in this region, and

415   a longer study is needed in the future.

416

417   **4. Conclusions**

418   This study presents observations of iodine oxide (IO) at the Indian Antarctic bases Maitri and

419   Bharati made over three summers from 2015 through 2017. IO was observed intermittently during

420   all the campaigns, with mixing ratios below 2 pptv. Using a profile retrieval algorithm, vertical

421   gradients of IO were estimated, and these showed a decreasing profile with a peak in the boundary

422   layer. The vertical profiles confirmed past hypothesis of a source from the ground considering a

423   sharp gradient. The vertical columns observed using the ground-based instrument are

424   approximately a factor of three-five higher than the climatological mean observed by the satellite,

425   which could be due to a difference in the measurement techniques and sensitivities. Airmass origin

426   analysis using back-trajectories did not lead to a conclusive answer about the source regions.

427   Indeed, it raises new questions on comparison with past observations, which show that we still do

428   not understand iodine chemistry in the polar regions. This study suggests that a longer dataset over

429   different seasons and regions of Antarctica is necessary to answer the outstanding questions

430   regarding the sources and seasonal importance of IO in the Indian Ocean sector of Antarctica.

431

5. Acknowledgements

433   We thank the logistical and scientific teams of the ISEA-34, ISEA-35, and ISEA-36 campaigns

434   for enabling observations through the expeditions. The ISEA campaigns are organised by the

435   National Centre for Polar and Ocean Research (NCPOR), Ministry of Earth Sciences (MOES),

436   Government of India. IITM and NCPOR are funded by MOES, Government of India.

6. Author contributions:

438   ASM conceptualised the research plan and methodology, did the analysis and wrote the

439   manuscript. MSB did the field observations. SB, TW, NB and ASL helped with the interpretation

440   of the observations and AS provided the satellite observations and helped interpret them.

441

7. References

442   Allan, J. D., Williams, P. I., Najera, J., Whitehead, J. D., Flynn, M. J., Taylor, J. W., Liu, D.,

443   Darbyshire, E., Carpenter, L. J., Chance, R., Andrews, S. J., Hackenberg, S. C. and McFiggans,

444   G.: Iodine observed in new particle formation events in the Arctic atmosphere during

445   ACCACIA, Atmos. Chem. Phys., 15(10), 5599–5609, doi:10.5194/acp-15-5599-2015, 2015.

446

447   Atkinson, H. M., Huang, R.-J., Chance, R., Roscoe, H. K., Hughes, C., Davison, B., Schönhardt,

448   A., Mahajan, A. S., Saiz-Lopez, A., Hoffmann, T. and Liss, P. S.: Iodine emissions from the sea

449   ice of the Weddell Sea, Atmos. Chem. Phys., 12, 11229–11244, doi:10.5194/acp-12-11229-

450   2012, 2012.

451   Barrie, L. A., Bottenheim, J. W., Schnell, R. C., Crutzen, P. J. and Rasmussen, R. A.: Ozone

452   destruction and photochemical reactions at polar sunrise in the lower Arctic atmosphere, Nature,

453   334(14), 138–141 [online] Available from:

454   http://www.nature.com/nature/journal/v334/n6178/abs/334138a0.html (Accessed 3 May 2012),

455   1988.

456   Beirle, S., Dörner, S., Donner, S., Remmers, J., Wang, Y. and Wagner, T.: The Mainz Profile

457   Algorithm (MAPA), Atmos. Meas. Tech. Discuss., 1–33, doi:10.5194/amt-2018-375, 2018.

458   Bogumil, K., Orphal, J., Homann, T., Voigt, S., Spietz, P., Fleischmann, O. C., Vogel, A.,

459   Hartmann, M., Kromminga, H., Bovensmann, H., Frerick, J. and Burrows, J. P.: Measurements

460   of molecular absorption spectra with the SCIAMACHY pre-flight model: instrument

461   characterization and reference data for atmospheric remote-sensing in the 230–2380 nm region,

462   J. Photochem. Photobiol. A Chem., 157(2–3), 167–184, doi:10.1016/S1010-6030(03)00062-5,

463   2003.

464   Bottenheim, J. W., Gallant, A. G. and Brice, K. A.: Measurements of NOy Species and O3 at 82-

465   Degrees-N Latitude, Geophys. Res. Lett., 13(2), 113–116, 1986.

466   Burrows, J. P., Hölzle, E., Goede, A. P. H., Visser, H. and Fricke, W.: SCIAMACHY – Scanning

467   Imaging Absorption Spectrometer for Atmospheric Chartography, Acta Astronaut., 35, 445–451,

468   1995.

469   Buys, Z., Brough, N., Huey, L. G., Tanner, D. J., von Glasow, R. and Jones, a. E.: High

470   temporal resolution Br2, BrCl and BrO observations in coastal Antarctica, Atmos. Chem. Phys.,

471   13, 1329–1343, doi:10.5194/acp-13-1329-2013, 2013.

472   Carpenter, L. J., Wevill, D. J., Palmer, C. J. and Michels, J.: Depth profiles of volatile iodine and

473   bromine-containing halocarbons in coastal Antarctic waters, Mar. Chem., 103, 227–236, 2007.

474   Carpenter, L. J., MacDonald, S. M., Shaw, M. D., Kumar, R., Saunders, R. W., Parthipan, R.,

475   Wilson, J. and Plane, J. M. C.: Atmospheric iodine levels influenced by sea surface emissions of

476   inorganic iodine, Nat. Geosci., 6(2), 108–111, doi:10.1038/ngeo1687, 2013.

477   Chance, K. V and Spurr, R. J.: Ring effect studies: Rayleigh scattering, including molecular

478   parameters for rotational Raman scattering, and the Fraunhofer spectrum., Appl. Opt., 36(21),

479   5224–5230 [online] Available from: http://www.ncbi.nlm.nih.gov/pubmed/18259337, 1997.

480   Cuevas, C. A., Maffezzoli, N., Corella, J. P., Spolaor, A., Vallelonga, P., Kjær, H. A., Simonsen,

481   M., Winstrup, M., Vinther, B., Horvat, C., Fernandez, R. P., Kinnison, D., Lamarque, J.-F.,

482   Barbante, C. and Saiz-Lopez, A.: Rapid increase in atmospheric iodine levels in the North

483   Atlantic since the mid-20th century, Nat. Commun., 9(1), 1452, doi:10.1038/s41467-018-03756-

484   1, 2018.

485 Deutschmann, T., Beirle, S., Frieß, U., Grzegorski, M., Kern, C., Kritten, L., Platt, U., Prados-

486 Román, C., Pukite, J., Wagner, T., Werner, B. and Pfeilsticker, K.: The Monte Carlo atmospheric

487 radiative transfer model McArtim: Introduction and validation of Jacobians and 3D features, J.

488 Quant. Spectrosc. Radiat. Transf., 112(6), 1119–1137, doi:10.1016/j.jqsrt.2010.12.009, 2011.

489 Draxler, R. and Rolph, G.: HYSPLIT (HYbrid Single Particle Lagrangian Integrated Tra-

490 jectory). Model access via NOAA ARL Ready, [online] Available from:

491 http://www.arl.noaa.gov/ready/ hysplit4.html, 2003.

492 Fayt, C. and Van Roozendael, M.: QDOAS 1.00. Software User Manual, [online] Available

493 from: http://uv-vis.aeronomie.be/software/QDOAS/, 2013.

494 Fernandez, R. P., Carmona-Balea, A., Cuevas, C. A., Barrera, J. A., Kinnison, D. E., Lamarque,

495 J., Blaszczak-Boxe, C., Kim, K., Choi, W., Hay, T., Blechschmidt, A., Schönhardt, A., Burrows,

496 J. P. and Saiz-Lopez, A.: Modeling the Sources and Chemistry of Polar Tropospheric Halogens

497 (Cl, Br, and I) Using the CAM-Chem Global Chemistry-Climate Model, J. Adv. Model. Earth

498 Syst., 11(7), 2259–2289, doi:10.1029/2019MS001655, 2019.

499 Fogelqvist, E. and Tanhua, T.: Iodinated C1-C4 hydrocarbons released from ice algae in

500 Antarctica BT - Naturally-Produced Organohalogens, edited by A. Grimvall and E. W. B. de

501 Leer, pp. 295–305, Springer Netherlands, Dordrecht., 1995.

502 Frieß, U., Wagner, T., Pundt, I., Pfeilsticker, K., Platt, U. and Friefi, U.: Spectroscopic

503 Measurements of Tropospheric Iodine Oxide at Neumayer Station, Antarctica, Geophys. Res.

504 Lett., 28(10), 1941–1944, 2001.

505 Frieß, U., Deutschmann, T., Gilfedder, B. S., Weller, R. and Platt, U.: Iodine monoxide in the

506   Antarctic snowpack, Atmos. Chem. Phys., 10(5), 2439–2456 [online] Available from:

507   http://www.atmos-chem-phys.net/10/2439/2010/, 2010.

508   Garrison, D. L. and Buck, K. R.: The biota of Antarctic pack ice in the Weddell sea and

509   Antarctic Peninsula regions, Polar Biol., 10(3), 211–219, doi:10.1007/BF00238497, 1989.

510   Gómez Martín, J. C., Spietz, P. and Burrows, J. P.: Spectroscopic studies of the I-2/O-3

511   photochemistry - Part 1: Determination of the absolute absorption cross sections of iodine oxides

512   of atmospheric relevance, J. Photochem. Photobiol. A - Chem., 176(1–3), 15–38,

513   doi:10.1016/j.jphotochem.2005.09.024, 2005.

514   Grilli, R., Legrand, M., Kukui, A., Méjean, G., Preunkert, S. and Romanini, D.: First

515   investigations of IO, BrO, and NO2 summer atmospheric levels at a coastal East Antarctic site

516   using mode-locked cavity enhanced absorption spectroscopy., Geophys. Res. Lett., 40(4), 791–

517   796, doi:10.1002/GRL.50154, 2013.

518   Hay, T.: MAX – DOAS measurements of bromine explosion events in McMurdo Sound ,

519   Antarctica, University of Canterbury., 2010.

520   Hollwedel, J., Wenig, M., Beirle, S., Kraus, S., Kühl, S., Wilms-Grabe, W., Platt, U. and

521   Wagner, T.: Year-to- Year Variability of Polar Tropospheric BrO as seen by GOME, Adv. Sp.

522   Res., 34, 804–808 [online] Available from: http://dx.doi.org/10.1016/j.asr.2003.08.060, 2004.

523   Hönninger, G., von Friedeburg, C. and Platt, U.: Multi axis differential optical absorption

524   spectroscopy (MAX-DOAS), Atmos. Chem. Phys., 4, 231–254, doi:10.5194/acp-4-231-2004,

525   2004.

526   Inamdar, S., Tinel, L., Chance, R., Carpenter, L. J., Sabu, P., Chacko, R., Tripathy, S. C., Kerkar,

A. U., Sinha, A. K., Bhaskar, P. V., Sarkar, A., Roy, R., Sherwen, T. T., Cuevas, C., Saiz-Lopez, A., Ram, K. and Mahajan, A. S.: Estimation of Reactive Inorganic Iodine Fluxes in the Indian and Southern Ocean Marine Boundary Layer, Atmos. Chem. Phys., 20(20), 12093–12114, doi:10.5194/acp-20-12093-2020, 2020.

Jin, Z., Charlock, T. P., Smith, W. L. and Rutledge, K.: A parameterization of ocean surface albedo, Geophys. Res. Lett., 31(22), 1–4, doi:10.1029/2004GL021180, 2004.

Koenig, T. K., Baidar, S., Campuzano-Jost, P., Cuevas, C. A., Dix, B., Fernandez, R. P., Guo, H., Hall, S. R., Kinnison, D., Nault, B. A., Ullmann, K., Jimenez, J. L., Saiz-Lopez, A. and Volkamer, R.: Quantitative detection of iodine in the stratosphere, Proc. Natl. Acad. Sci., (15), 201916828, doi:10.1073/pnas.1916828117, 2020.

Kreher, K., Johnston, P. V., Wood, S. W., Nardi, B. and Platt, U.: Ground-based measurements of tropospheric and stratospheric BrO at Arrival Heights, Antarctica, Geophys. Res. Lett., 24(23), 3021–3024, doi:10.1029/97GL02997, 1997.

Legrand, M., McConnell, J. R., Preunkert, S., Arienzo, M., Chellman, N., Gleason, K., Sherwen, T., Evans, M. J. and Carpenter, L. J.: Alpine ice evidence of a three-fold increase in atmospheric iodine deposition since 1950 in Europe due to increasing oceanic emissions, Proc. Natl. Acad. Sci., 115(48), 12136–12141, doi:10.1073/pnas.1809867115, 2018.

Lewis, T. R., Gómez Martín, J. C., Blitz, M. A., Cuevas, C. A., Plane, J. M. C. and Saiz-Lopez, A.: Determination of the absorption cross sections of higher-order iodine oxides at 355 and 532 nm, Atmos. Chem. Phys., 20(18), 10865–10887, doi:10.5194/acp-20-10865-2020, 2020.

Mahajan, A. S., Shaw, M., Oetjen, H., Hornsby, K. E., Carpenter, L. J., Kaleschke, L., Tian-

548 Kunze, X., Lee, J. D., Moller, S. J., Edwards, P. M., Commane, R., Ingham, T., Heard, D. E. and

549 Plane, J. M. C.: Evidence of reactive iodine chemistry in the Arctic boundary layer, J. Geophys.

550 Res., 115(D20303,), doi:dx.doi.org/10.1029/2009JD013665, 2010.

551 Mahajan, A. S., Gómez Martín, J. C., Hay, T. D., Royer, S.-J., Yvon-Lewis, S. A., Liu, Y., Hu,

552 L., Prados-Román, C., Ordóñez, C., Plane, J. M. C. and Saiz-Lopez, A.: Latitudinal distribution

553 of reactive iodine in the Eastern Pacific and its link to open ocean sources, Atmos. Chem. Phys.,

554 12, 11609–11617, doi:10.5194/acp-12-11609-2012, 2012.

555 Mahajan, A. S., Tinel, L., Hulswar, S., Cuevas, C. A., Wang, S., Ghude, S., Naik, R. K., Mishra,

556 R. K., Sabu, P., Sarkar, A., Anilkumar, N. and Saiz Lopez, A.: Observations of iodine oxide in

557 the Indian Ocean marine boundary layer: A transect from the tropics to the high latitudes, Atmos.

558 Environ. X, 1, 100016, doi:10.1016/j.aeaoa.2019.100016, 2019.

559 Meller, R. and Moortgat, G. K.: Temperature dependence of the absorption cross sections of

560 formaldehyde between 223 and 323 K in the wavelength range 225-375 nm, J. Geophys. Res.,

561 105(D6), 7089–7101 [online] Available from: http://dx.doi.org/10.1029/1999JD901074, 2000.

562 O'Dowd, C. D., Facchini, M. C., Cavalli, F., Ceburnis, D., Mircea, M., Decesari, S., Fuzzi, S.,

563 Yoon, Y. J., Putaud, J. P. and Dowd, C. D. O.: Biogenically driven organic contribution to

564 marine aerosol, Nature, 431(7009), 676–680, doi:10.1038/nature02970.1., 2004.

565 Oltmans, S. J. and Komhyr, W. D.: Surface Ozone Distributions and Variations from 1973-1984

566 Measurements at the Noaa Geophysical Monitoring for Climatic-Change Base-Line

567 Observatories, J. Geophys. Res. - Atmos., 91(D4), 5229–5236, 1986.

568 Perovich, D. K., Grenfell, T. C., Light, B. and Hobbs, P. V.: Seasonal evolution of the albedo of

569   multiyear Actic sea ice, J. Geophys. Res. C Ocean., 107(10), doi:10.1029/2000jc000438, 2002.

570   Platt, U. and Stutz, J.: Differential optical absorption spectroscopy: Principles and applications,

571   First Edit., Springer., 2008.

572   Prakash Chaubey, J., Krishna Moorthy, K., Suresh Babu, S. and S. Nair, V.: The optical and

573   physical properties of atmospheric aerosols over the Indian Antarctic stations during southern

574   hemispheric summer of the International Polar Year 2007ĝ€"2008, Ann. Geophys., 29(1), 109–

575   121, doi:10.5194/angeo-29-109-2011, 2011.

576   Raso, A. R. W., Custard, K. D., May, N. W., Tanner, D., Newburn, M. K., Walker, L., Moore, R.

577   J., Huey, L. G., Alexander, L., Shepson, P. B. and Pratt, K. A.: Active molecular iodine

578   photochemistry in the Arctic, Proc. Natl. Acad. Sci. U. S. A., 114(38), 10053–10058,

579   doi:10.1073/pnas.1702803114, 2017.

580   Reifenhäuser, W. and Heumann, K. G.: Determinations of methyl-iodine in the antarctic

581   atmosphere at the south polar sea, Atmos. Environ. Part a-General Top., 26(16), 2905–2912,

582   1992.

583   Richter, A., Wittrock, F., Ladstätter-Weißenmayer, A. and Burrows, J. P.: GOME measurements

584   of stratospheric and tropospheric BrO, Adv. Sp. Res., 29(11), 1667–1672, 2002.

585   Rothman, L. S., Gordon, I. E., Babikov, Y., Barbe, A., Chris Benner, D., Bernath, P. F., Birk,

586   M., Bizzocchi, L., Boudon, V., Brown, L. R., Campargue, A., Chance, K., Cohen, E. a., Coudert,

587   L. H., Devi, V. M., Drouin, B. J., Fayt, A., Flaud, J.-M., Gamache, R. R., Harrison, J. J.,

588   Hartmann, J.-M., Hill, C., Hodges, J. T., Jacquemart, D., Jolly, A., Lamouroux, J., Le Roy, R. J.,

589   Li, G., Long, D. a., Lyulin, O. M., Mackie, C. J., Massie, S. T., Mikhailenko, S., Müller, H. S. P.,

590   Naumenko, O. V., Nikitin, A. V., Orphal, J., Perevalov, V., Perrin, A., Polovtseva, E. R.,

591   Richard, C., Smith, M. a. H., Starikova, E., Sung, K., Tashkun, S., Tennyson, J., Toon, G. C.,

592   Tyuterev, V. G. and Wagner, G.: The HITRAN 2012 molecular spectroscopic database, J. Quant.

593   Spectrosc. Radiat. Transf., 130, 4–50, doi:10.1016/j.jqsrt.2013.07.002, 2013.

594   Saiz-Lopez, A. and Blaszczak-boxe, C. S.: The polar iodine paradox, Atmos. Environ., 145, 72–

595   73, doi:10.1016/j.atmosenv.2016.09.019, 2016.

596   Saiz-Lopez, A. and von Glasow, R.: Reactive halogen chemistry in the troposphere., Chem. Soc.

597   Rev., doi:10.1039/c2cs35208g, 2012.

598   Saiz-Lopez, A., Mahajan, A. S., Salmon, R. A., Bauguitte, S. J.-B., Jones, A. E., Roscoe, H. K.

599   and Plane, J. M. C.: Boundary Layer Halogens in Coastal Antarctica, Science (80-.)., 317(5836),

600   348–351, doi:10.1126/science.1141408, 2007a.

601   Saiz-Lopez, A., Chance, K. V., Liu, X., Kurosu, T. P. and Sander, S. P.: First observations of

602   iodine oxide from space, Geophys. Res. Lett., 34(12), L12812, doi:10.1029/2007GL030111,

603   2007b.

604   Saiz-Lopez, A., Plane, J. M. C., Mahajan, A. S., Anderson, P. S., Bauguitte, S. J.-B., Jones, A.

605   E., Roscoe, H. K., Salmon, R. A., Bloss, W. J., Lee, J. D. and Heard, D. E.: On the vertical

606   distribution of boundary layer halogens over coastal Antarctica: implications for O-3, HOx, NOx

607   and the Hg lifetime, Atmos. Chem. Phys., 8(4), 887–900, 2008.

608   Saiz-Lopez, A., Plane, J. M. C., Baker, A. R., Carpenter, L. J., von Glasow, R., Martín, J. C. G.,

609   McFiggans, G. B., Saunders, R. W. and Gómez Martín, J. C.: Atmospheric Chemistry of Iodine,

610   Chem. Rev., 112(3), 1773–1804, doi:10.1021/cr200029u, 2012.

611   Saiz-Lopez, A., Blaszczak-Boxe, C. S. and Carpenter, L. J.: A mechanism for biologically-

612   induced iodine emissions from sea-ice, Atmos. Chem. Phys., 15, 9731–9746, doi::10.5194/acp-

613   15-9731-2015, 2015a.

614   Saiz-Lopez, A., Baidar, S., Cuevas, C. A., Koenig, T. K., Fernandez, R. P., Dix, B., Kinnison, D.

615   E., Lamarque, J., Rodriguez-Lloveras, X., Campos, T. L. and Volkamer, R.: Injection of iodine

616   to the stratosphere, Geophys. Res. Lett., 42, 6852–6859, doi:10.1002/2015GL064796, 2015b.

617   Schönhardt, A., Richter, A., Wittrock, F., Kirk, H., Oetjen, H., Roscoe, H. K. and Burrows, J. P.:

618   Observations of iodine monoxide (IO) columns from satellite, Atmos. Chem. Phys., 8, 637–653

619   [online] Available from: http://hal-insu.archives-ouvertes.fr/hal-00296438/ (Accessed 30 April

620   2012), 2008.

621   Schönhardt, A., Begoin, M., Richter, a., Wittrock, F., Kaleschke, L., Gómez Martín, J. C. and

622   Burrows, J. P.: Simultaneous satellite observations of IO and BrO over Antarctica, Atmos.

623   Chem. Phys., 12(14), 6565–6580, doi:10.5194/acp-12-6565-2012, 2012.

624   Stutz, J., Kim, E. S., Platt, U., Bruno, P., Perrino, C. and Febo, A.: UV-visible absorption cross

625   sections of nitrous acid, J. Geophys. Res., 105(D11), 14585–14592, 2000.

626   Thalman, R. and Volkamer, R. A.: Temperature Dependent Absorption Cross-Sections of O2-O2

627   collision pairs between 340 and 630 nm and at atmospherically relevant pressure, Phys. Chem.

628   Chem. Phys., 15, 15371–15381, doi:10.1039/C3CP50968K, 2013.

629   Theys, N., Van Roozendael, M., Hendrick, F., Yang, X., De Smedt, I., Richter, A., Begoin, M.,

630   Errera, Q., Johnston, P. V., Kreher, K. and De Mazière, M.: Global observations of tropospheric

631   BrO columns using GOME-2 satellite data, Atmos. Chem. Phys., 11, 1791–1811,

632   doi:10.5194/acp-11-1791-2011, 2011.

633   Tuckermann, M., Ackermann, R., Golz, C., LorenzenSchmidt, H., Senne, T., Stutz, J., Trost, B.,

634   Unold, W., Platt, U. and Lorenzen-Schmidt, H.: DOAS-observation of halogen radical-catalysed

635   arctic boundary layer ozone destruction during the ARCTOC-campaigns 1995 and 1996 in Ny-

636   Alesund, Spitsbergen, Tellus B, 49B(5), 533–555, 1997.

637   Vallelonga, P., Maffezzoli, N., Moy, A. D., Curran, M. A. J., Vance, T. R., Edwards, R., Hughes,

638   G., Barker, E., Spreen, G., Saiz-Lopez, A., Corella, J. P., Cuevas, C. A. and Spolaor, A.: Sea-ice-

639   related halogen enrichment at Law Dome, coastal East Antarctica, Clim. Past, 13(2), 171–184,

640   doi:10.5194/cp-13-171-2017, 2017.

641   Vandaele, A. C., Hermans, C., Simon, P., Carleer, M. R., Colins, R., Fally, F., Merienne, M. F.,

642   Jenouvrier, A. and Coquart, B.: Measurements of NO2 absorption cross-sections at 42000 cm-1

643   to 10000 cm-1 (238-1000 nm) at 220 K and 298 K, J. Quant. Spectrosc. Radiat. Transf., 59, 171–

644   184, 1997.

645   Vandaele, A. C., Hermans, C., Simon, P. C., Carleer, M., Colin, R., Fally, S., Merienne, M. F.,

646   Jenouvrier, A. and Coquartii, B.: Measurements od the NO2 absorption cross-section from 42000

647   cm-1 to 10000 cm-1 (238-1000 nm) at 220 K and 294 K, J. Quant. Spectrosc. Radiat. Transf.,

648   59(3), 171–184, 1998.

649   Wagner, T., Leue, C., Wenig, M., Pfeilsticker, K. and Platt, U.: Spatial and temporal distribution

650   of enhanced boundary layer BrO concentrations measured by the GOME instrument aboard

651   ERS-2, J. Geophys. Res. - Atmos., 106(D20), 24225–24235, 2001.

652   Wagner, T., Dix, B., Friedeburg, C. V., Frieß, U., Sanghavi, S., Sinreich, R. and Platt, U.: MAX-

653   DOAS O 4 measurements: A new technique to derive information on atmospheric aerosols—

654   Principles and information content, J. Geophys. Res., 109(D22), doi:10.1029/2004JD004904,

655   2004.

656   Wagner, T., Beirle, S. and Deutschmann, T.: Three-dimensional simulation of the Ring effect in

657   observations of scattered sun light using Monte Carlo radiative transfer models, Atmos. Meas.

658   Tech., 2(1), 113–124, doi:10.5194/amt-2-113-2009, 2009.

659   Wagner, T., Apituley, A., Beirle, S., Dörner, S., Friess, U., Remmers, J. and Shaiganfar, R.:

660   Cloud detection and classification based on MAX-DOAS observations, Atmos. Meas. Tech.,

661   7(5), 1289–1320, doi:10.5194/amt-7-1289-2014, 2014.

662   Wagner, T., Beirle, S., Benavent, N., Bösch, T., Chan, K. L., Donner, S., Dörner, S., Fayt, C.,

663   Frieß, U., García-Nieto, D., Gielen, C., González-Bartolome, D., Gomez, L., Hendrick, F.,

664   Henzing, B., Jin, J. L., Lampel, J., Ma, J., Mies, K., Navarro, M., Peters, E., Pinardi, G.,

665   Puentedura, O., Puķīte, J., Remmers, J., Richter, A., Saiz-Lopez, A., Shaiganfar, R., Sihler, H.,

666   Van Roozendael, M., Wang, Y. and Yela, M.: Is a scaling factor required to obtain closure

667   between measured and modelled atmospheric O<sub>4</sub>

668   absorptions? An assessment of uncertainties of measurements and radiative transfer simulations

669   for 2 selected days during th, Atmos. Meas. Tech., 12(5), 2745–2817, doi:10.5194/amt-12-2745-

670   2019, 2019.

671

672

673   Figures

674
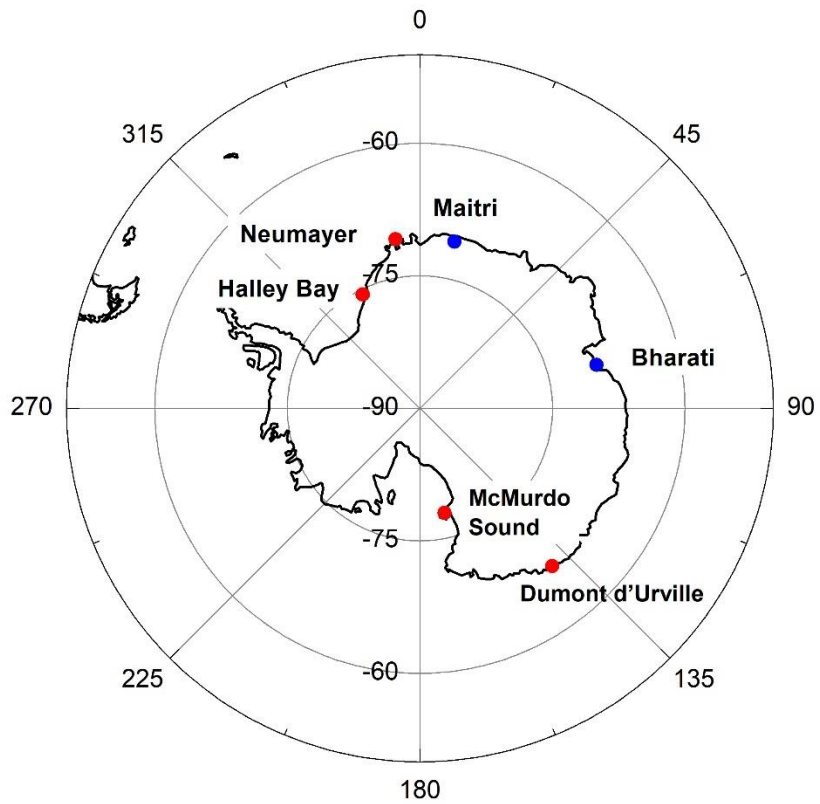
Figure 1: Map showing the location of the two Indian Antarctic stations, Maitri and Bharati, where

676   observations of IO were performed during this study (blue dots). Previous locations that have

677   reported observations of IO are also marked on the map (red dots).

678
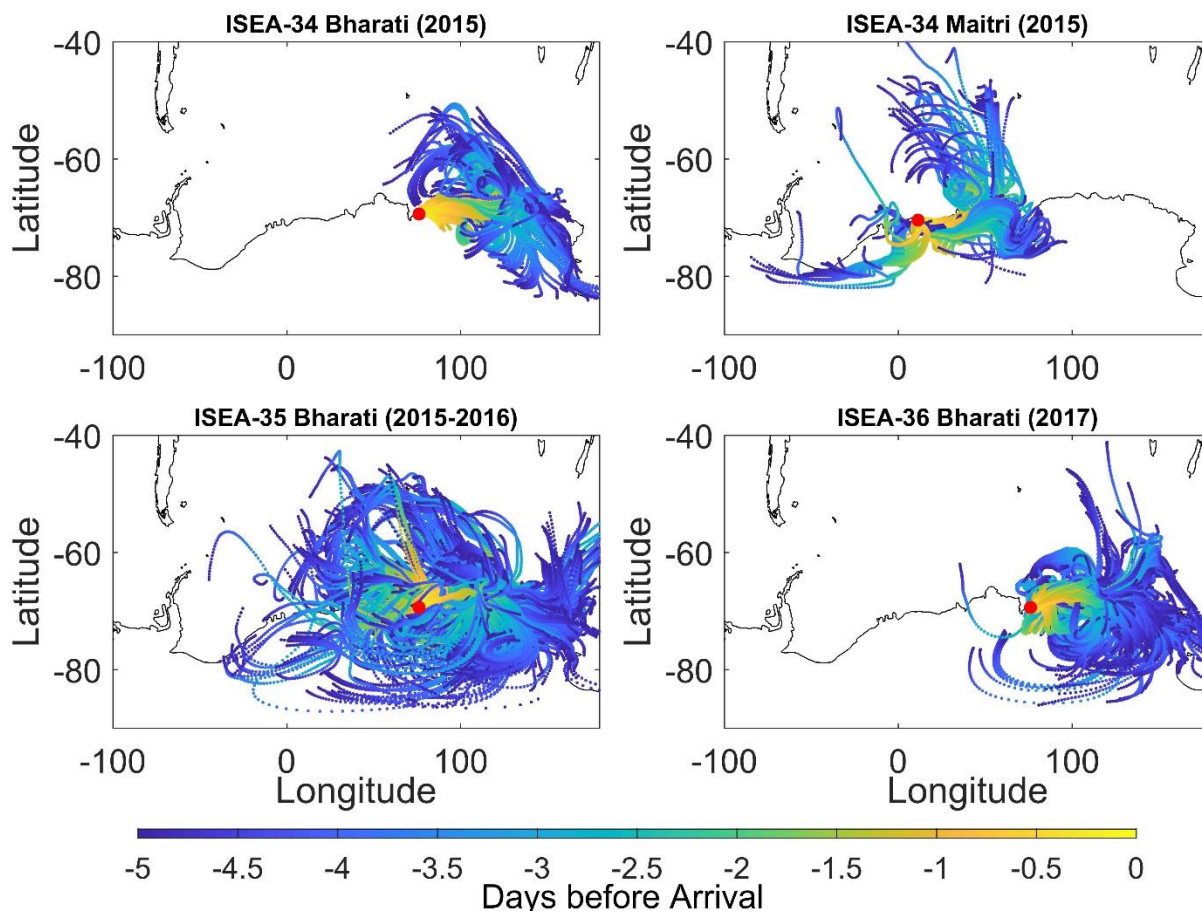
Figure 2: 5-day back-trajectories arriving at the two stations on the days that the measurements of IO were conducted as a part of the 34th, 35th and 36th ISEA expeditions are shown. The back-trajectories were calculated using the HYbrid Single-Particle Lagrangian Integrated Trajectory (HYSPLIT) model, arriving every hour (Draxler and Rolph, 2003).

685
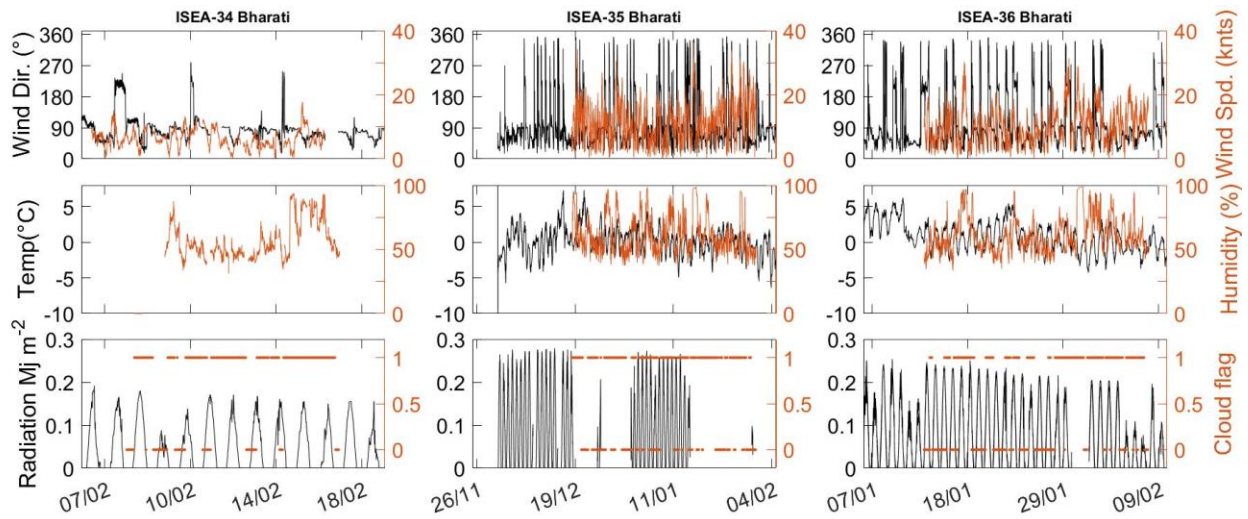
Figure 3: Observations of different meteorological parameters that were measured during the various summer campaigns are shown here. The top panels show the wind direction and speed; the middle panels show the temperature and humidity; and the bottom panels show the radiation and cloudiness (1 is defined as 30% cloudy skies and above). Observations of these parameters were not made during the 34th ISEA at Maitri and the gaps indicate instrumental or observational issues. The data had a time resolution of 5 min.

692

693
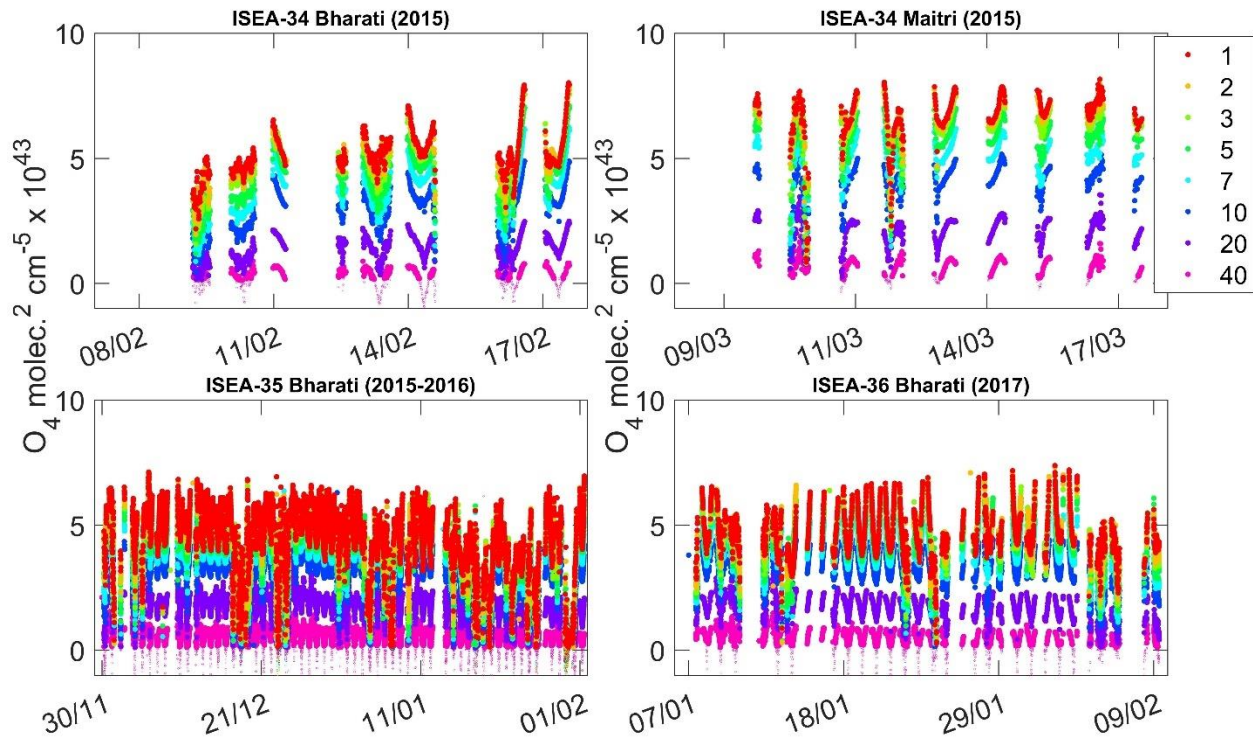
Figure 4: O$_4$ DSCDs observed during the four campaigns are shown. The empty circles represent

values below the 2σ detection limit of the instrument, while the filled circles are values above the

2σ detection limit. The data are color-coded according to elevation angles.

697

698
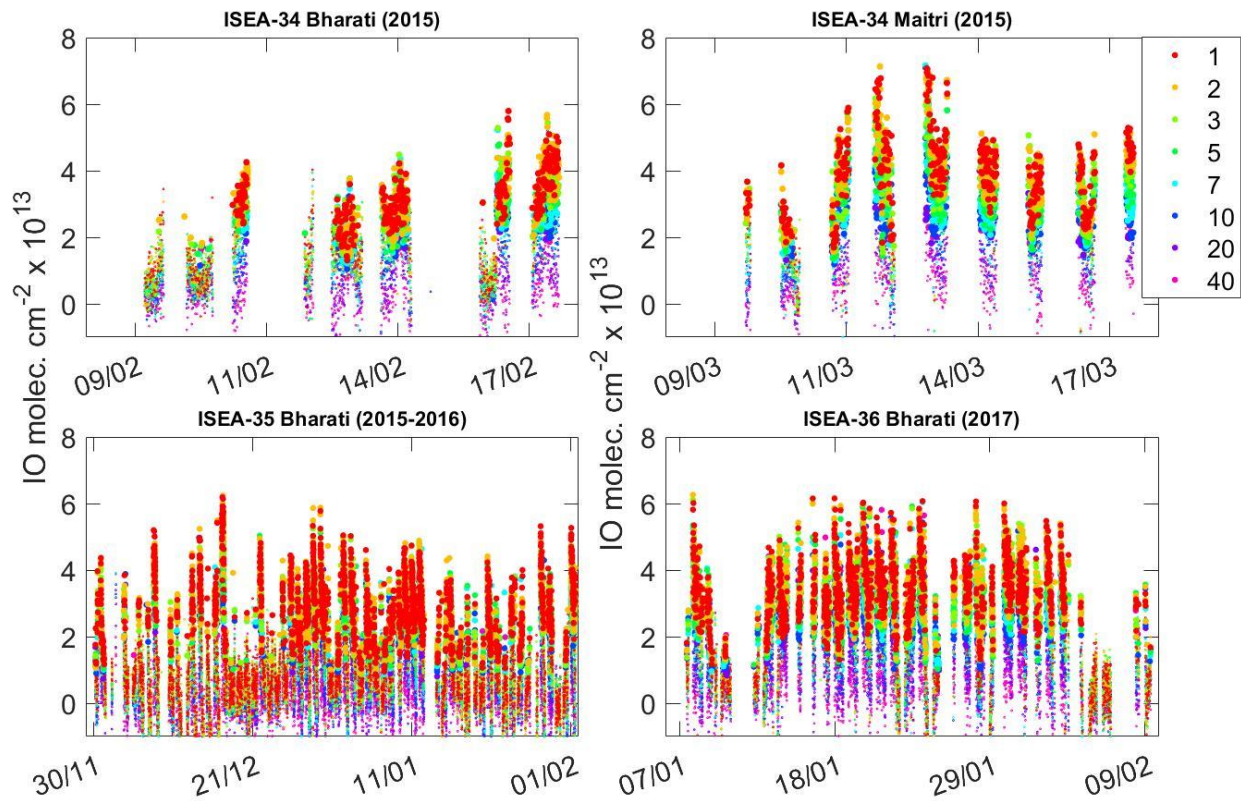
Figure 5: IO DSCDs observed during the four campaigns are shown. The smaller circles represent

values below the 2σ detection limit of the instrument, while the bigger circles are values above the

2σ detection limit. The data are color-coded according to elevation angles.

702

703

704
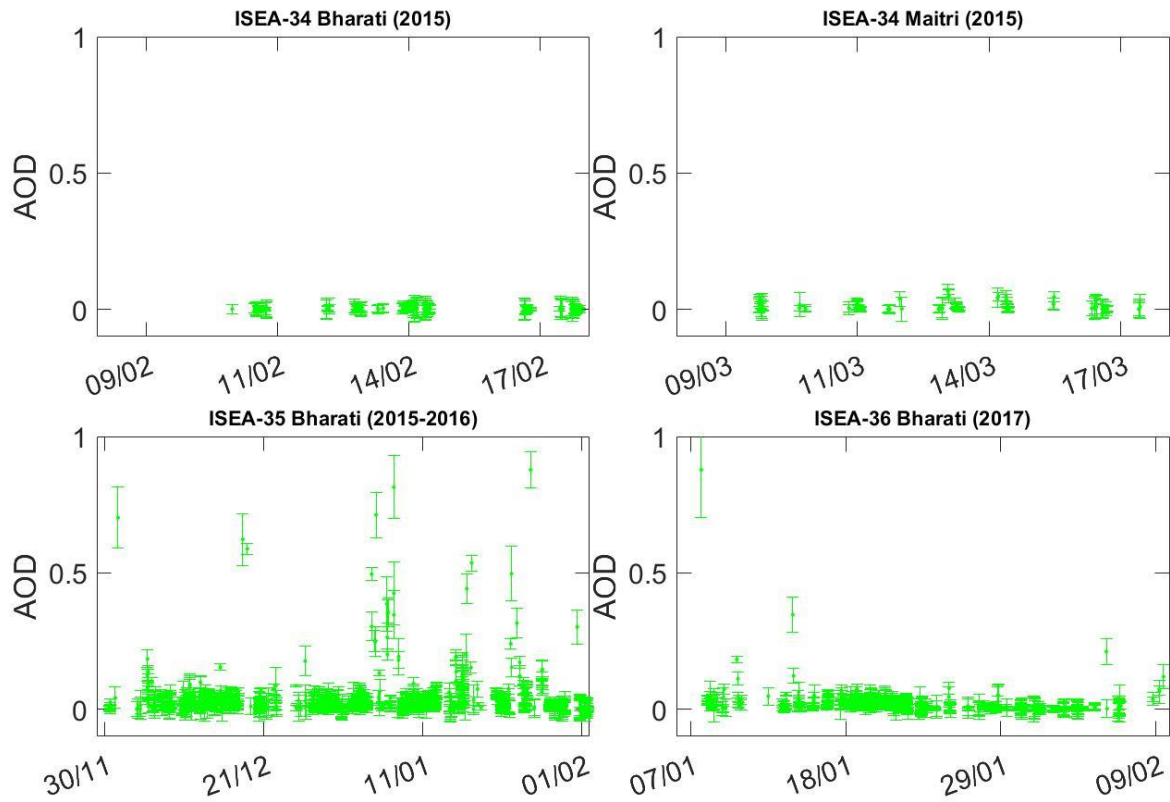
Figure 6: AOD timeseries retrieved using the O_4 DSCDs for all the four campaigns are shown. The data show only the 'good' datapoints, which are reliable and were mostly during clear sky conditions.

708
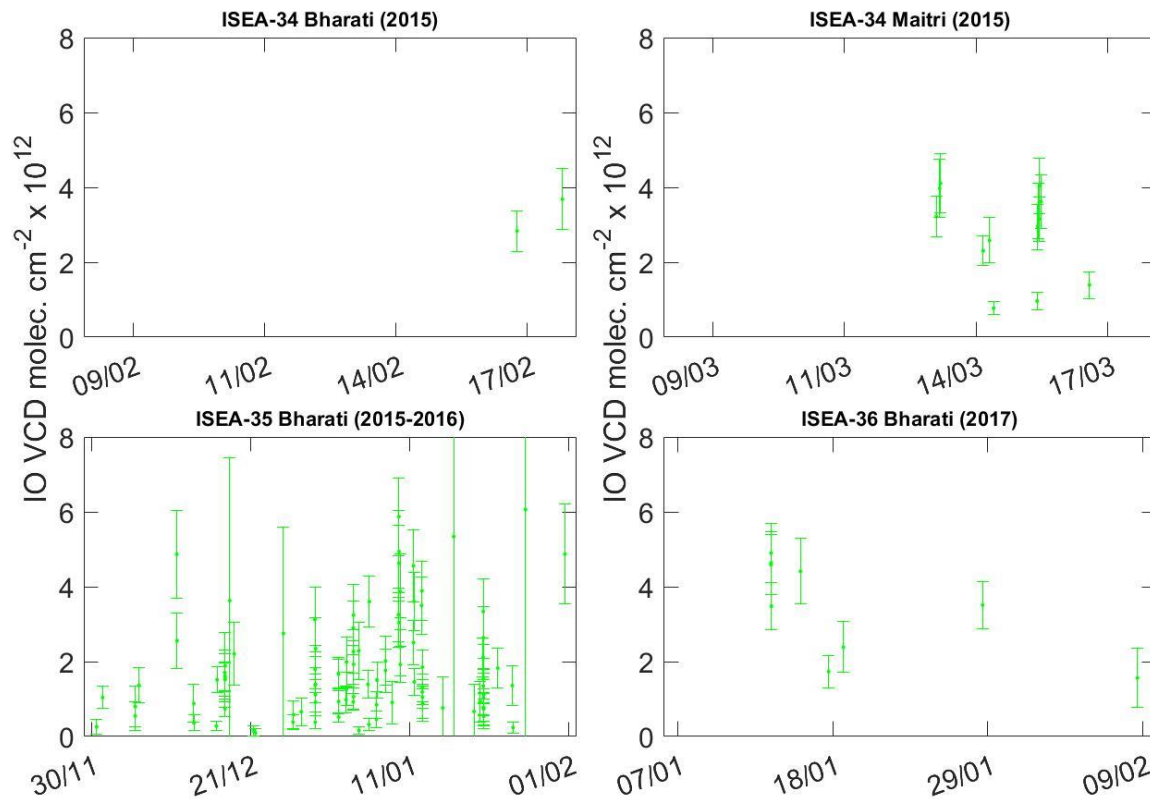
709

710   **Figure 7:** Observations of IO vertical column densities observed through all the four campaigns

711   are shown. These data were mostly during periods of clear sky, and where IO was observed above

712   the detection limit for most of the set elevation angles, enabling a reliable profile retrieval.

713

714
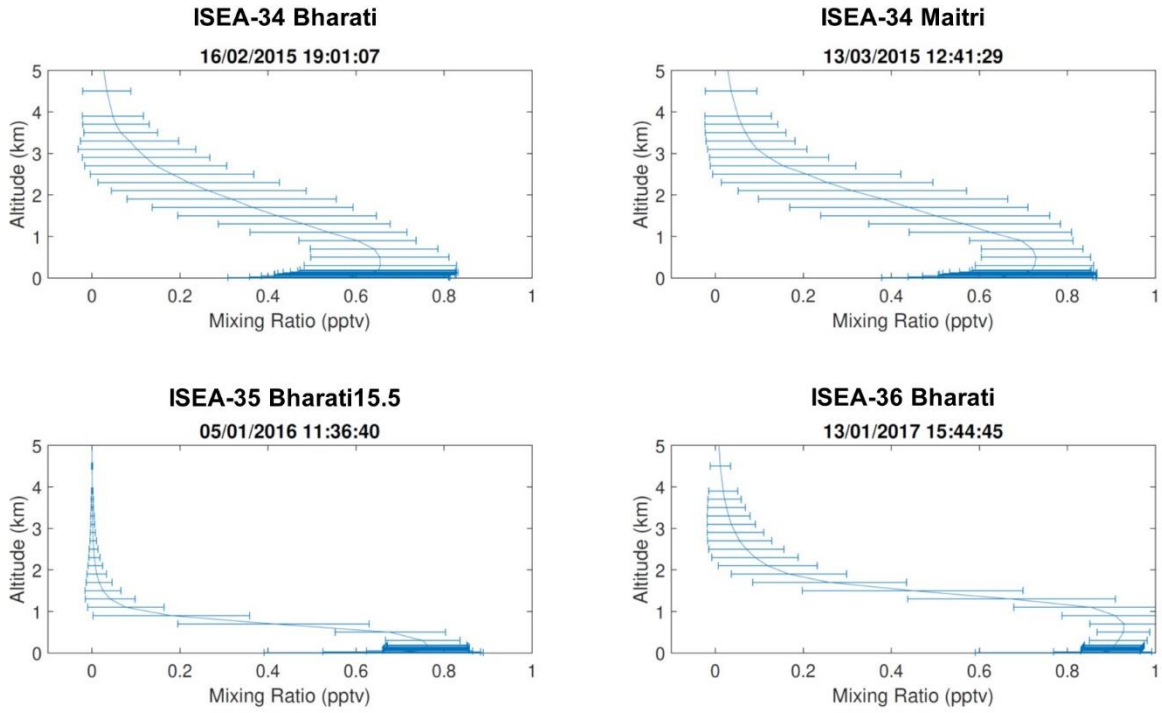
Figure 8: Typical examples of IO vertical profiles retrieved during all the four campaigns are

shown.

717

718
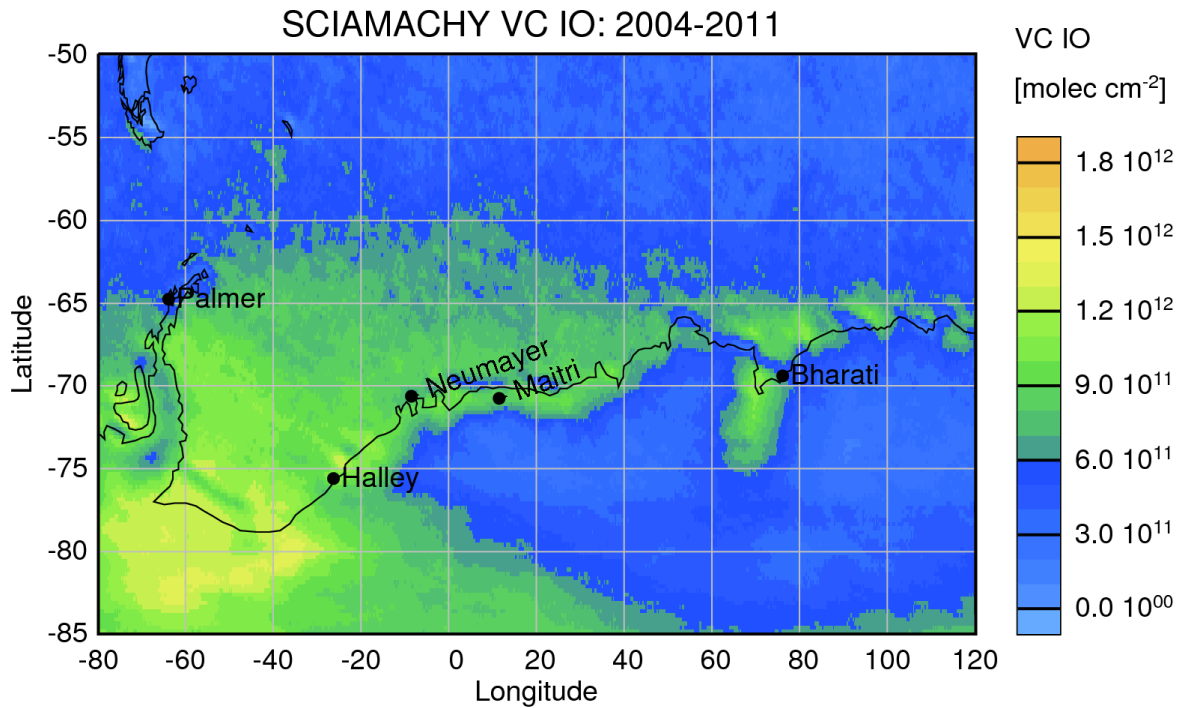
Figure 9: Averaged VCDs of IO as retrieved by SCIAMACHY between 2004-2011are shown.

Observations suggest that lower levels of IO are expected at Bharati and Maitri, as compared to

Halley Bay and Neumayer.

722

723
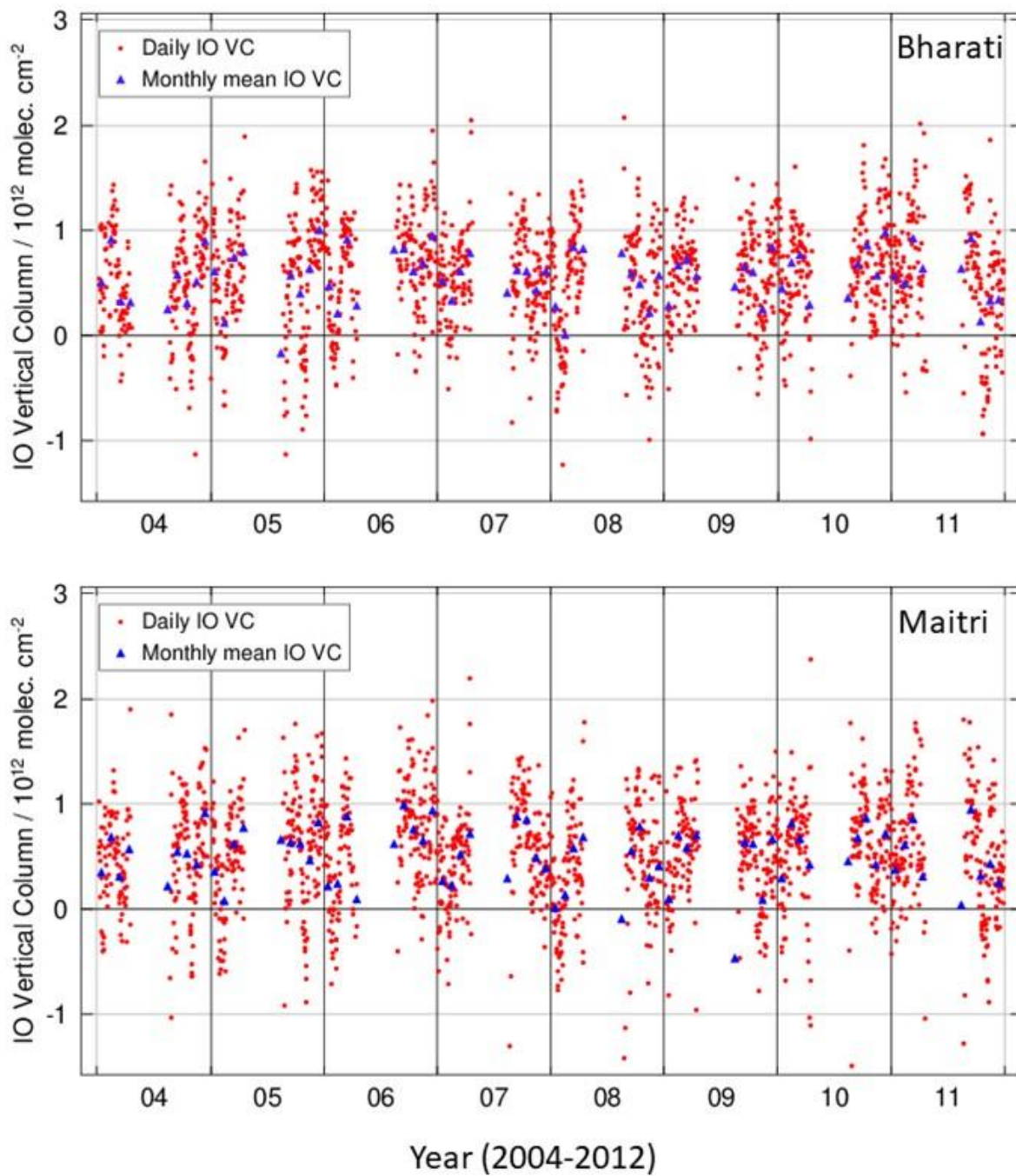
Figure 10: Timeseries of IO VCD observations at the Bharati station as retrieved by SCIAMACHY. The monthly mean values are shown in blue, and the daily datapoints are shown in red.

727